PHOTONICS Research

Mimicking the gravitational effect with gradient index lenses in geometrical optics

Wen Xiao, Sicen Tao, and Huanyang Chen*

Institute of Electromagnetics and Acoustics and Department of Physics, Xiamen University, Xiamen 361005, China
**Corresponding author: kenyon@xmu.edu.cn*

Received 5 January 2021; revised 19 April 2021; accepted 19 April 2021; posted 19 April 2021 (Doc. ID 418787); published 8 June 2021

General relativity establishes the equality between matter-energy density and the Riemann curvature of spacetime. Therefore, light or matter will be bent or trapped when passing near the massive celestial objects, and Newton's second law fails to explain it. The gravitational effect is not only extensively studied in astronomy but also attracts a great deal of interest in the field of optics. People have mimicked black holes, Einstein's ring, and other fascinating effects in diverse optical systems. Here, with a gradient index lens, in the geometrical optics regime, we mimic the Schwarzschild precession in the orbit of the star S2 near the Galactic Center massive black hole, which was recently first detected by European Southern Observatory. We also find other series of gradient index lenses that can be used to mimic the possible Reissner–Nordström metric of Einstein's field equation and dark matter particle motion. Light rays in such gradient lenses will be closed in some cases, while in other cases it would be trapped by the center or keep dancing around the center. Our work presents an efficient toy model to help investigate some complex celestial behaviors, which may require long period detection by using high-precision astronomical tools. The induced gradient lenses enlightened by the gravitational effect also enrich the family of absolute optical instruments for their selective closed trajectories.

https://doi.org/10.1364/PRJ.418787

1. INTRODUCTION

Einstein's general theory of relativity is one of the cornerstones in modern physics. It holds the best understanding of gravity so far, explaining that the nature of universal gravitation originates from matter-energy, resulting in curved spacetime. To date, general relativity (GR) has passed all the experimental tests with flying colors, such as the precession of Mercury [1], gravitational redshift [2], the observations of solar-mass pulsars in binary systems [3], and the gravitational waves from several stellar mass, black hole candidate in-spirals [4]. Recently, the report of first detection of the Schwarzschild precession in S2's orbit around the nearest massive black hole (candidate) in the Galaxy Center has received attention, being more prominent evidence of GR [5]. In optics, in analogy to the equality between matter-energy and curved spacetime, macroscopic Maxwell's equations in complex inhomogeneous media can be mapped into free-space Maxwell's equations of an arbitrary spacetime metric [6–10], leading to lots of transformation optical applications like invisibility cloaks [11–17], field rotators [18,19], and illusion devices [20]. Moreover, despite the functionality of controlling the flow of light, this analogy has also been utilized to mimic some exciting gravitational effects related to GR in return, for instance, black holes [21–27], Einstein's ring [28], de Sitter space [29,30], and cosmic strings [31,32].

For the above mimicking, most works are from the perspective of transformation optics. However, in classical aspect, the analogy has another inherent correspondence, revealed through the least action principle in mechanics (Maupertuis's principle) and Fermat's principle in geometrical optics. This correspondence is also called optical-mechanical analogy [33–36]. It means that we can observe some gravitational phenomena in the regime of geometrical optics using light rays. Comparing the forms of Hamilton equations in these two fields, one can obtain the closed connection between classical mechanics and geometrical optics, i.e., the potential V and total energy E (of unit mass) can construct a gradient refractive index profile n, with the same shape of trajectories in both mechanics and geometrical optics [36]. Here, based on the optical-mechanical analogy, in the geometrical optics regime, we use a gradient index lens to mimic the star S2's Schwarzschild precession near the Galactic Center massive black hole SgrA* mentioned above. With the help of light ray trajectories in the gradient index lens, the difference between universal gravitation and GR is clearly shown. The extra cubic term r^{-3} in the effective potential of the Schwarzschild spacetime makes the path in precession and causes Newton's second law to fail [37]. Moreover, inspired by such mimicking, we propose two other types of gradient index lenses stemming from the Newton and Hooke potentials,

each with an additional quadratic perturbation r^{-2}. The orbits in those lenses will not always be in precession. It can be closed under certain conditions or be trapped by the center. Such gravitational effects of additional quadratic term systems in astronomy are possibly related to the charged Reissner–Nordström metric [38,39] of GR and the dark matter particle motions in galaxies [40].

2. SCHWARZSCHILD PRECESSION MIMICKING

The nearest black hole candidate SgrA* is located at the center of the Milky Way, surrounded by a very dense cluster of stars. One of the closest stars is S2, whose distance from SgrA* at orbit's perihelion is about 120Au (Au, atomic units). Due to the extreme gravity environment, the system of SgrA* provides a wonderful "laboratory" for GR testing. For the star S2, the orbit obeys the Schwarzschild metric of Einstein's field equation:

$$\mathrm{d}s^2 = -\left(1-\frac{2GM}{c^2 r}\right)^{-1}\mathrm{d}r^2 - r^2\mathrm{d}\theta^2 - r^2\sin^2\theta\mathrm{d}\phi^2 + c^2\left(1-\frac{2GM}{c^2 r}\right)\mathrm{d}t^2, \tag{1}$$

where G is gravitational constant, M is the mass of SgrA*, and c is the speed of light. The geodesic equations in this curved spacetime are

$$\frac{\mathrm{d}^2 x^\alpha}{\mathrm{d}s^2} + \Gamma^\alpha_{\mu\nu}\frac{\mathrm{d}x^\mu}{\mathrm{d}s}\frac{\mathrm{d}x^\nu}{\mathrm{d}s} = 0, \tag{2}$$

where α, μ, and ν traverse all generalized coordinates (r, θ, ϕ, t), and $\Gamma^\alpha_{\mu\nu}$ is called the Christoffel symbol, which can be calculated by the metric tensor in Eq. (1). Equation (2) contains four equations related to the four generalized coordinates. By the spherical symmetry, and without any loss of generality, we chose $\theta = \frac{\pi}{2}$ as the plane of trajectory. Then the derivatives of θ vanish and the equations are reduced to three. When we substitute values of $\Gamma^\alpha_{\mu\nu}$, these equations are

$$\left(\frac{\mathrm{d}r}{\mathrm{d}\tau}\right)^2 + r^2\left(\frac{\mathrm{d}\phi}{\mathrm{d}\tau}\right)^2\left(1-\frac{2GM}{c^2 r}\right) - c^2\left(1-\frac{2GM}{c^2 r}\right)^2 \times \left(\frac{\mathrm{d}t}{\mathrm{d}\tau}\right)^2 + c^2\left(1-\frac{2GM}{c^2 r}\right) = 0, \tag{3}$$

$$\frac{\mathrm{d}^2\phi}{\mathrm{d}\tau^2} + \frac{2}{r}\frac{\mathrm{d}r}{\mathrm{d}\tau}\frac{\mathrm{d}\phi}{\mathrm{d}\tau} = 0, \tag{4}$$

$$\frac{\mathrm{d}^2 t}{\mathrm{d}\tau^2} + \frac{2GM}{c^2 r^2}\left(1-\frac{2GM}{c^2 r}\right)^{-1}\frac{\mathrm{d}r}{\mathrm{d}\tau}\frac{\mathrm{d}t}{\mathrm{d}\tau} = 0, \tag{5}$$

where $\mathrm{d}s = c\mathrm{d}\tau$. Equation (4) can be rewritten as $r^2\frac{\mathrm{d}\phi}{\mathrm{d}\tau} = L$ (L is a constant), stating that angular momentum is conserved. Combining Eqs. (3) and (5), another key equation about energy conservation can be found. The two dominant equations are the following:

$$\left(\frac{\mathrm{d}r}{\mathrm{d}\tau}\right)^2 + r^2\left(\frac{\mathrm{d}\phi}{\mathrm{d}\tau}\right)^2 - \frac{2GM}{r} = -c^2(1-K^2) + \frac{2GMr}{c^2}\left(\frac{\mathrm{d}\phi}{\mathrm{d}\tau}\right)^2, \tag{6}$$

$$r^2\frac{\mathrm{d}\phi}{\mathrm{d}\tau} = L, \tag{7}$$

where K is also an integration constant. After some algebraic calculation, Eqs. (6) and (7) will be simplified into one formula:

$$c^2K^2 - c^2 = \left(\frac{\mathrm{d}r}{\mathrm{d}t}\right)^2 + \frac{L^2}{r^2} - \frac{2GM}{r} - \frac{2GML^2}{c^2 r^3}. \tag{8}$$

That is the final equation of the matter motion in Schwarzschild spacetime. In Newtonian mechanics, a particle with mass m and total energy E, influenced only by the gravity from a spherically symmetric object with mass M, satisfies

$$\frac{2E}{m} = \left(\frac{\mathrm{d}r}{\mathrm{d}t}\right)^2 + \frac{L^2}{r^2} - \frac{2GM}{r}. \tag{9}$$

The first two terms on the right side of Eq. (9) correspond to kinetic energy part, and the third term corresponds to the potential. Comparing Eq. (9) with Eq. (8), one can find that both left sides of the equations represent per unit mass of the total energy, and their difference is that the Schwarzschild metric of GR has an additional cubic potential item r^{-3}. When r is small, the cubic item dominates, yet the potential in origin will more rapidly approach infinity, causing the precession of perihelion in orbits. Therefore, interestingly, the potential form $V = -\frac{GM}{r} - \frac{GML^2}{c^2 r^3}$ can be regarded as a modified universal gravitational potential of celestial bodies on behalf of the impact of GR, at least in the mathematical form.

Now let us treat the mechanical problem in the geometrical optics regime using a gradient index lens. To begin, we employ the closed relationship between classical mechanics and geometrical optics based on the optical-mechanical analogy. The shape of particle trajectories in mechanics is the same as the trajectories of light rays in a lens with a refractive index distribution [36]

$$n = \sqrt{2(E-V)}, \tag{10}$$

and E and V in Eq. (10) are the total energy per unit mass and the potential, respectively. Equation (10) indicates that the gradient index lens is determined by E and V. In celestial mechanics, E and V dominate the matter energy distribution of the system, and when it comes to geometrical optics, these two key factors are reflected in the refractive index profile n, where n plays the major role in light ray propagation. One must notice that in the analogy, the independent variables of two fields are not the same. Maupertuis's principle (the least action principle) is $\int mv\mathrm{d}l$, and the Fermat's principle is $\int n\mathrm{d}l$. It seems that refractive index profile n is the role of "velocity" v in mechanics [n has the dimension of v in Eq. (10)]. However, if the independent variable in optics corresponds to the physical time t, the refractive index n will be proportional to the speed of light c. Thus, the independent variable of the optics under the analogy is actually a stepped parameter, not the physical time t. Here we will use ζ to distinguish it from t. To further identify the mechanical problem in optics, we must know the initial condition or another important physical quantity, the orbital angular momentum L, of both fields.

For star S2, the per unit mass energy and per unit orbital angular momentum are $E = -\frac{GM}{2a}$ and $L = \sqrt{GMa(1-e^2)}$,

respectively. Here a is semi-major axis and e is the eccentricity of the orbit. From Ref. [5], $a = 1031.32$Au, $e = 0.884649$, and thus the perihelion $r_p = a(1-e) = 118.922$Au. The mass of the nearest black hole candidate SgrA* is $M = 4.261 \times 10^6 M_s$ (M_s is the solar mass). The Schwarzschild precession of per S2's orbit can be obtained from GR as $\Delta\phi = \frac{3\pi R_s}{a(1-e^2)} = 12.1'$, where $R_s = \frac{2GM}{c^2}$ is the Schwarzschild radius. With the help of the optical-mechanical analogy, this precession of star S2 can be visualized vividly in a gradient index lens. Substitute $E = -\frac{GM}{2a}$ and modified universal gravitational potential $V = -\frac{GM}{r} - \frac{GML^2}{c^2 r^3}$ into Eq. (10), and the refractive index profile mimicking Schwarzschild precession induced by the black hole SgrA* is $n = \sqrt{2\left(-\frac{GM}{2a} + \frac{GM}{r} + \frac{GML^2}{c^2 r^3}\right)}$. In fact, there are several other mimickings about static black holes, such as $n = \frac{1}{r}$ [22,23,26]. However, the gradient lens we propose based on the optical-mechanical analogy is very different from those in the previous works. The lens here is a general formula for interactions between two massive celestial bodies, not limited to black holes. Our method involves the astronomical quantities, which is more reasonable in revealing the actual celestial motions in the universe, while the mimicking $n = \frac{1}{r}$ is emphasized on the trapping effect, and it is more suitable for a light absorber, or we can call it an "optical black hole." In Fig. 1(a), we draw the light ray trajectories of both universal gravitation analogy and Schwarzschild precession analogy. The massive black hole is placed in the origin, and the trajectories start at the perihelion $(0, -r_p)$ indicated by the cyan spot below the origin. The direction of velocity is perpendicular to the radius vector at that point. The universal gravitation analogy is shown in a red dashed elliptically closed curve, while the blue curve represents the mimicking of Schwarzschild precession. From Fig. 1(a), it can be found that the precession accumulates and becomes obvious with the evolution of the "time" ζ. At the beginning, the two curves are very close to each other, and after 15 periods the difference is gradually revealed. Although ζ does not correspond to the physical time t, the shapes of the trajectories in mechanics as well as the precession per orbit ($\Delta\phi$) are conserved in the geometrical optics [33]. Therefore, if we care less about the physical time, this mimicking is fast and effective to make some useful predictions at first, by avoiding the complex mathematical calculations of the metric of curved spacetime.

In Fig. 1(a) we enlarge a small area (the white dashed box) to show the precession clearly. The precession looks very small as depicted in the inset (in the right corner). However, it is much bigger compared with the precession of Mercury around the Sun. We also extract the x and y components of universal gravitation analogy (red curve) and Schwarzschild precession analogy (blue curve). The results are presented in Figs. 1(a) and 1(b), respectively. We show the last three periods and find that the separation between universal gravitation and Schwarzschild precession is obvious in the plot of $x(\zeta)$. The separation is getting larger as the "time" ζ increases.

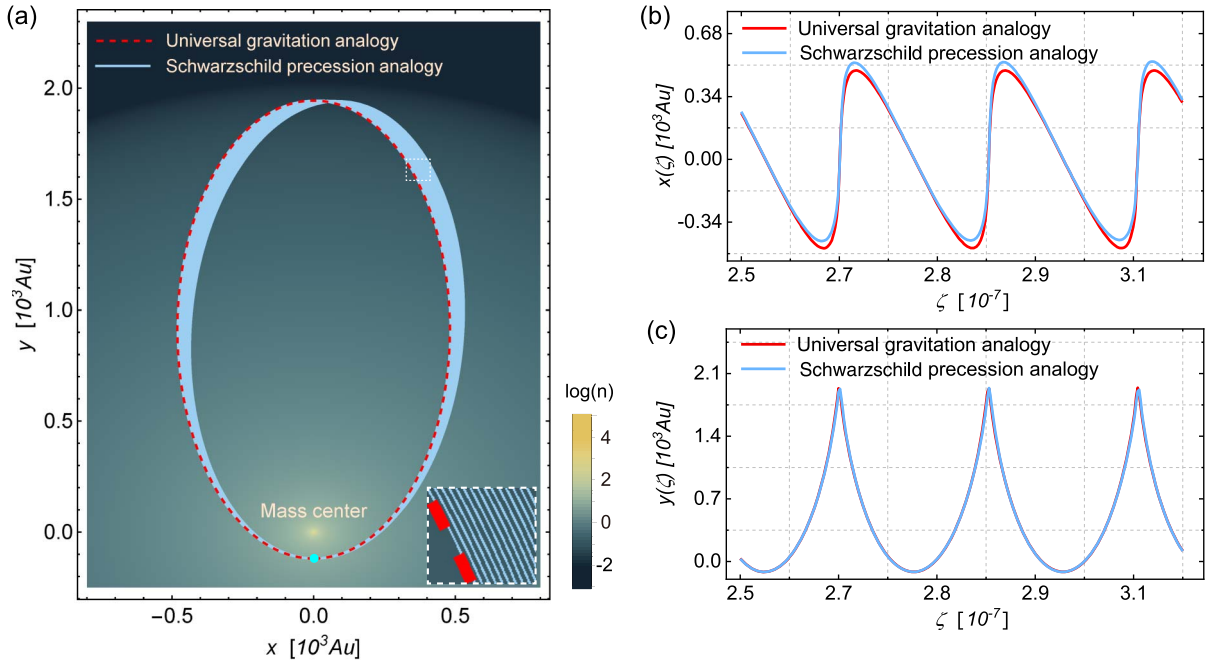

Fig. 1. (a) Light ray trajectories of universal gravitation analogy and Schwarzschild precession analogy of the star S2's orbit around the nearest massive black hole SgrA* candidate (in the origin). Trajectories start from the perihelion $(0, -r_p)$ (the cyan dot), and $r_p = a(1-e) = 118.922$Au. The red dashed elliptically closed curve is the analogy of universal gravitation. The blue curve varying with the "time" ζ is the mimicking of Schwarzschild precession. Per orbit of this precession is 12.1′, and here it is about 3° for 15 periods. The inset in the lower right corner is an enlarged view of the trajectories in the upper dashed white box. The background color map is the logarithmic refractive index distribution $\log(n)$ of the induced gradient lens mimicking Schwarzschild precession. The profile $n(r)$ goes infinitely at the origin, and it equals 0 in the region outside $r = 2.063$Au [the plotted minimum value $\log(n) = -3$ here]. (b) and (c) The x components and y components of these two trajectories, respectively. Three periods are plotted, and the difference between universal gravitation and Schwarzschild precession is clearly shown in curves of $x(\zeta)$.

However, the curves of $y(\zeta)$ remain almost the same due to the high eccentricity of the orbit.

3. PERTURBATION OF QUADRATIC TERM r^{-2}

In the previous section, the Schwarzschild precession is successfully reproduced in geometrical optics based on the optical-mechanical analogy. The modified universal gravitational potential is the key role in connecting mechanics with optics. In the vast universe, there are various kinds of effective potentials that describe the interaction between celestial bodies. Some effective potentials can be adopted to represent the influence of GR if the spacetime is static, like the Schwarzschild metric and the Reissner–Nordström metric. In this section, we are interested in whether there exist other potentials in astronomy that can make a different trajectory, not always in the elliptical orbit or in precession. In this way, the novel gravitational effects in celestial mechanics may enlighten us to meet some new ideas for optics based on the optical-mechanical analogy. In Schwarzschild precession, it is the cubic term r^{-3} that yields the precession of the perihelion and causes the orbit to no longer be closed. However, if the additional term in the modified potential is quadratic, i.e., r^{-2}, will the phenomenon in the corresponding gradient index lens be the same as Schwarzschild precession? The answer here is no. For convenience, we consider a more concise and basic potential form in Newton mechanics, i.e., $V=-\frac{1}{r}$, to manifest gravity. Now we add the extra quadratic term r^{-2} with coefficient λ and make up a new modified Newton potential $V=-\frac{1}{r}-\frac{\lambda}{r^2}$. In mechanics, the trajectory of a particle (set the mass as unit) under such a central potential field can be precisely solved, and the expression is [37]

$$r=\frac{\alpha^2L^2}{1+\sqrt{1+\frac{2E\alpha^2}{L^2}}\cos(\alpha\theta)}, \tag{11}$$

where θ is polar angle, and $\alpha=\sqrt{1-\frac{2\lambda}{L^2}}$, which depends on coefficient λ and orbital angular momentum L. According to Eq. (10), the refractive index profile of the "quadratic" gradient lens is $n=\sqrt{2\left(E+\frac{1}{r}+\frac{\lambda}{r^2}\right)}$. It is noticed that if $E=-\frac{1}{2}$, $\lambda=0$, this lens is the well-known Eaton lens with the profile $n=\sqrt{\frac{2}{r}-1}$ [41], which is widely used in optics for bending the desired angle of input rays. According to the optical-mechanical analogy, the Eaton lens is connected to the Newton profile $V=-\frac{1}{r}$, and the trajectories in that lens are also ellipses, the same as the red dashed curve in Fig. 1(a). Besides, the Eaton lens is also an important self-imaging lens in the optical absolute instrument family. Before we start the exploration of light rays in the "quadratic" lens, the initial condition, i.e., the orbital angular momentum L in mechanics must be changed to the proper form in the geometrical optics. The L in geometrical optics is determined by the location and the refractive index profile of the ray [42]:

$$L=n(r)r\sin\psi, \tag{12}$$

where ψ is the angle between the radius vector and the tangent of the ray trajectory. Here, we also set $E=-\frac{1}{2}$ to keep consistent with the Eaton lens (for $n=1$ at $r=1$ in the Eaton lens). We divide the "quadratic" modified Newton lens into two cases of $\lambda>0$ and $\lambda<0$ and plot several typical examples in Fig. 2.

In Fig. 2, the light rays start from point (1, 0) with different launching angle ψ, stating their various orbit angular momentum L. The first row is the case of $\lambda=1$, with $\psi=\frac{3}{4}\pi$ and $\psi=\frac{1}{3}\pi$ in Figs. 2(a) and 2(b), respectively. The trajectory in Fig. 2(a) is trapped by the center, with a pure imaginary value of α ($\alpha=\frac{\sqrt{3}}{3}i$), while the trajectory in Fig. 2(b) is closed. It has finished passing through the origin three times, and then it finally joins into the starting point. The value of α is $\frac{1}{3}$. However, the situations in the case of the negative λ are different, as shown in Figs. 2(c) and 2(d). For $\lambda=-\frac{6}{37}$, the trajectories of the light rays have clear boundaries. They are stably restricted in an annular region with the positive refractive index. The ray in Fig. 2(c) with a launching angle $\psi=\frac{1}{6}\pi$ is in precession and keeps dancing around the center. Its α is equal to $\frac{\sqrt{73}}{5}$. The ray in Fig. 2(d) with the initial angle $\psi=\frac{1}{4}\pi$ is closed in a petaloid shape, and the α equals $\frac{7}{5}$. The closed trajectory has seven petals and passes through the origin five times. The reason why the trajectories are in various shapes can be dated back to Eq. (11) (the path solution in mechanics). The value of factor α before the polar angle θ is essential. If α is rational, taking the form of $\frac{p}{q}$ (p, q are coprime integers), the trajectory will be repeated and closed after the period $2q\pi$. Recalling the closed trajectories in this part [$\alpha=\frac{1}{3}$ in Fig. 2(b) and $\alpha=\frac{7}{5}$ in Fig. 2(d)], we find that light rays will have p petals and travel the origin q times for $\alpha=\frac{p}{q}$. We call it the general rule of closed orbits. Nevertheless, if α is nonrational, there is no finite period, and it will keep dancing around the center as illustrated in Fig. 2(c) ($\alpha=\frac{\sqrt{73}}{5}$). And as for the nonreal α, the term $\cos(\alpha\theta)$ in Eq. (11) will change into hyperbolic cosine form, which is further away from the period function. Thus the ray will collapse to straight the center if the launching direction is toward the center [Fig. 2(a)], or it will travel for some distance and turn back to the center due to the reflection resulting from the gradually decreasing n (in mechanics the turning point is due to the vanishing velocity) if the launching direction is opposite to the center.

In fact, the phenomena for the case $\lambda<0$ in quadratic modified Newton potential $V=-\frac{1}{r}-\frac{\lambda}{r^2}$ of Figs. 2(c) and 2(d) are related to another exact metric of Einstein's field equation, i.e., the Reissner–Nordström metric. This metric describes the spacetime around a spherically symmetric nonrotating massive body with an electric charge Q. If Q is zero, it reduces to the Schwarzschild metric. However, if the electric charge Q is nonzero, the charged particle motion has additional quadratic item r^{-2}, along with the fourth power item r^{-4} in Eq. (8), whereas the higher power term can be neglected in some ways, and thus the situation is fundamentally similar to Figs. 2(c) and 2(d).

4. MODEL EXTENSION

The above Newton profile $V=-\frac{1}{r}$ is a basic potential in universe. Another common potential, the Hooke potential $V=\frac{1}{2}r^2$ (also named the harmonic potential) also supports

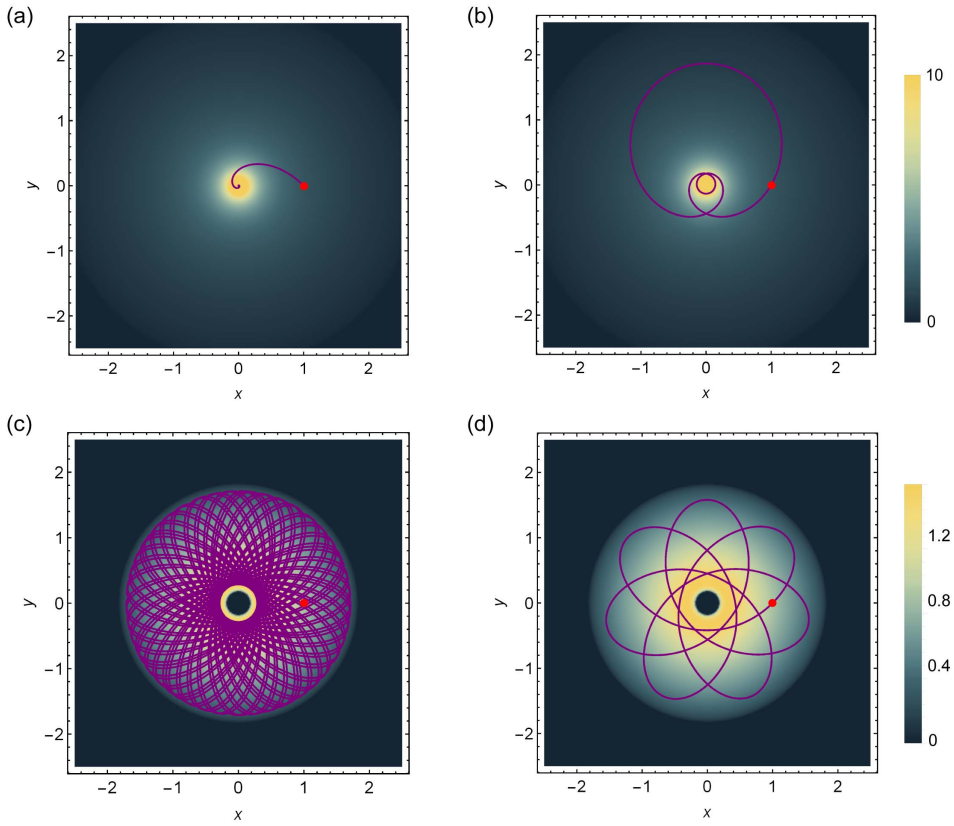

Fig. 2. Light ray trajectories in the lens $n(r)=\sqrt{2\left(E+\frac{1}{r}+\frac{\lambda}{r^2}\right)}$ with $E=-\frac{1}{2}$ induced by the modified Newton potential of two different λ. The color maps show the corresponding distributions of the refractive index profiles. All the rays start from point (1, 0), as indicated by the red dot. First row: $\lambda=1$; (a) and (b) correspond to the launching angles $\psi=\frac{3}{4}\pi$ and $\psi=\frac{1}{3}\pi$, respectively. (a) The ray collapses into the center, like the trapping effect of a black hole. α equals $\frac{\sqrt{3}}{3}i$, which is a pure imaginary number. (b) The ray is closed after traveling around the origin three times, with $\alpha=\frac{1}{3}$. Second row: $\lambda=-\frac{6}{37}$; (c) and (d) represent the launching angles $\psi=\frac{1}{6}\pi$ and $\psi=\frac{1}{4}\pi$, respectively. (c) The trajectory is in precession and keeps dancing around the center, where α is $\frac{\sqrt{73}}{5}$. (d) The closed ray trajectory of seven rotational symmetric petals. It joins into the starting point after traveling around the origin five times, and α is $\frac{7}{5}$.

closed elliptical trajectories, which can describe the gravitation of dark matter particles within the spherical isotropic homogeneous galaxies [40]. With the optical-mechanical analogy, the Hooke potential is associated with the Luneburg lens $n=\sqrt{2-r^2}$ [43], with the energy constant $E=1$. The Luneburg lens is also a perfect imaging lens and has extensive applications in optical antennas. Now this begs the question: if the quadratic term $\frac{\lambda}{r^2}$ is introduced into the Hooke potential, how does the light ray behave in its induced gradient index lens?

To solve this problem, we can first search its orbit in mechanics, and then transform the quantities in the language of optics based on the analogy. By the laws of conservation of energy and momentum, the trajectory of the particle in the modified Hooke potential $V=\frac{1}{2}r^2-\frac{\lambda}{r^2}$ can be solved as [37]

$$r^2=\frac{\alpha^2L^2/E}{1+\sqrt{1-\frac{\alpha^2L^2}{E^2}}\cos(2\alpha\theta)}, \tag{13}$$

where α is also the intermediate parameter and $\alpha=\sqrt{1-\frac{2\lambda}{L^2}}$. Equation (13) expounds that when α is rational ($\alpha=p/q$), the trajectories will be closed, whereas, as the factor in front of the polar angle θ is 2α, the trajectory will obey the general rule based on 2α. Different from the energy (with unit mass) in a Newtonian system, the energy of the modified Hooke potential is positive, and we also set $E=1$ to be in accordance with the Luneburg lens. By using Eq. (10), the problem can be mimicked by the gradient index lens, i.e., $n=\sqrt{2\left(1-\frac{1}{2}r^2+\frac{\lambda}{r^2}\right)}$. We also calculate two cases of $\lambda>0$ and $\lambda<0$ in geometrical optics, and the results are shown in Fig. 3.

There are two closed trajectories in Figs. 3(b) and 3(d). Their shapes are exactly consistent with the general rule of closed orbits. In Fig. 3(b), the value of 2α is $\frac{7}{4}$, and thus the trajectory has seven petals and passes the origin four times, while for $2\alpha=8$ in Fig. 3(d), the trajectory has eight petals after traveling around the origin one time. Besides, the analysis of the trapping effect in Fig. 3(a) and the precession in Fig. 3(c) is the same as that in the previous section. It should be noted that the parameters of λ and ψ can be arbitrary, and those we chose are to better evidence our consequences. The trajectories in these two types of lenses (induced by the modified Newton potential and Hooke potential) are pretty interesting. The lenses can perform a

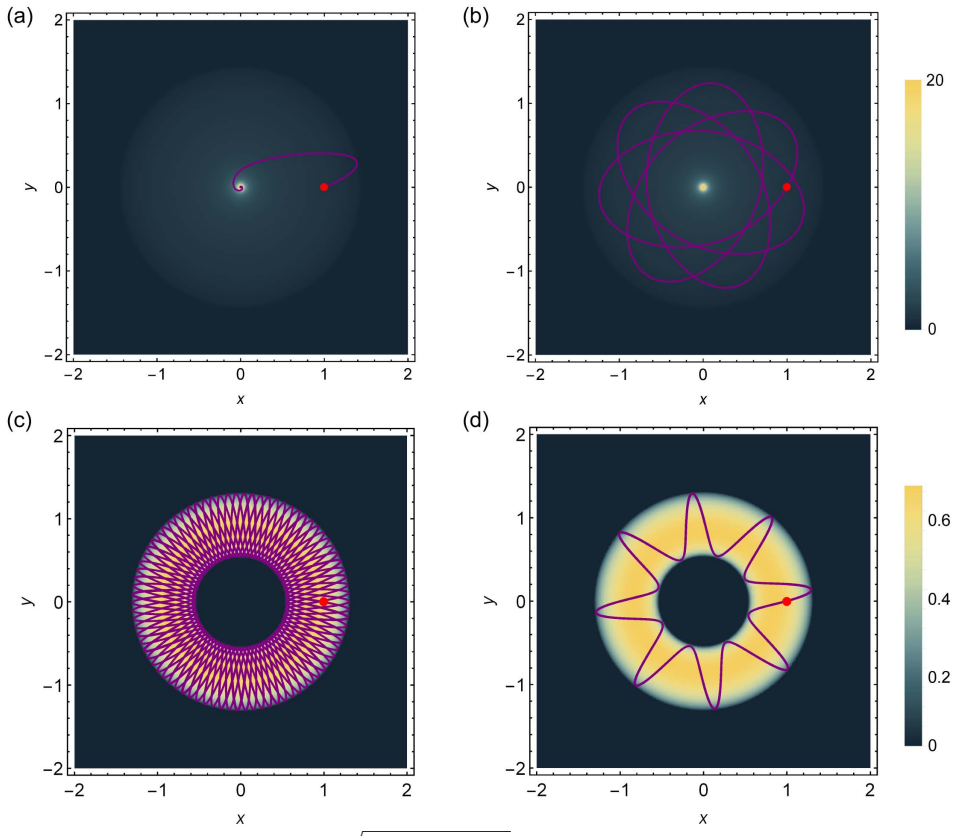

Fig. 3. Light ray trajectories in the gradient lens $n(r) = \sqrt{2\left(E - \frac{1}{2}r^2 + \frac{\lambda}{r^2}\right)}$ with $E = 1$ induced by the modified Hooke potential of two different λ. The color maps and color bars indicate the refractive index profiles. Rays start from the point (1, 0) (in red dot). First row: $\lambda = \frac{45}{422}$. (a) $\psi = \frac{1}{8}\pi$. Trapping effect of the center with $\alpha = i\sqrt{-1 + \frac{45}{256}\csc^2\left(\frac{\pi}{8}\right)}$. The ray first travels some distance towards the positive x direction and finally turns back to the center. (b) $\psi = \frac{1}{3}\pi$. Closed trajectory with seven petals. It travels around the center four times and $2\alpha = \frac{7}{4}$. Second row: $\lambda = \frac{15(2-\sqrt{3})}{2(-34+15\sqrt{3})}$. (c) $\psi = \frac{17}{18}\pi$, and α is an nonrational number herein. The orbit is in precession and restricted in an annular region. (d) $\psi = \frac{1}{12}\pi$. The closed ray path has only eight petals with $2\alpha = 8$.

"selective imaging (self-imaging)" in optics, as only certain sets of the light rays following the general rule can be closed. Thus it can be regarded as a special kind of optical absolute instrument, as their conditions for imaging are restricted. Moreover, the trapping effect and the precessional motion may also have potential applications in light absorbing and confining (cavity), and these effects are more common in such lenses.

5. CONCLUSION

In this paper, we propose a gradient refractive index lens to mimic the Schwarzschild precession in the orbit of star S2 near the Galactic Center massive black hole SgrA* for the first time to our knowledge, based on the optical-mechanical analogy in the field of geometrical optics. The optical-mechanical analogy involves potential V and energy E of the system, and thus we use a modified universal gravitational potential to represent the influence of GR. Inspired by the Schwarzschild precession mimicking, we propose two types of gradient lenses stemming from the modified Newton potential and modified Hooke potential, which are possibly related to the Reissner–Nordström metric and dark matter motions in astronomy. With the help of ray tracing, we find the light trajectories in these lenses will be closed, governed by a general rule, otherwise they will be trapped by the center or be continuously in precession. These interesting properties can be utilized in designing selective optical imaging devices and light absorbers. The optical-mechanical analogy builds a useful bridge to connect mechanics with optics, and our work shows some of its capabilities. Such interdisciplinary work of celestial mechanics and optics promises to potentially enlighten us with some new thoughts and ideas for both fields, for example, the Eaton lens, the Luneburg lens, and the Morse lens in optics [44].

Funding. National Natural Science Foundation of China (92050102, 11874311); National Key Research and Development Program of China (2020YFA0710100); Fundamental Research Funds for the Central Universities (20720200074).

Disclosures. The authors declare no conflicts of interest.

REFERENCES

1. A. Einstein, "The foundation of the general theory of relativity," Ann. Phys. **354**, 769–822 (1916).

2. J. C. Hafele and R. E. Keating, "Around-the-world atomic clocks: predicted relativistic time gains," Science **177**, 166–168 (1972).
3. M. Kramer, I. H. Stairs, R. N. Manchester, M. A. McLaughlin, A. G. Lyne, R. D. Ferdman, M. Burgay, D. R. Lorimer, A. Possenti, N. D'Amico, J. M. Sarkissian, G. B. Hobbs, J. E. Reynolds, P. C. C. Freire, and F. Camilo, "Tests of general relativity from timing the double pulsar," Science **314**, 97–102 (2006).
4. B. P. Abbott, R. Abbott, T. D. Abbott, M. R. Abernathy, F. Acernese, K. Ackley, C. Adams, T. Adams, P. Addesso, R. X. Adhikari, V. B. Adya, C. Affeldt, M. Agathos, K. Agatsuma, N. Aggarwal, O. D. Aguiar, L. Aiello, A. Ain, P. Ajith, B. Allen, A. Allocca, P. A. Altin, S. B. Anderson, W. G. Anderson, K. Arai, M. A. Arain, M. C. Araya, C. C. Arceneaux, J. S. Areeda, N. Arnaud, K. G. Arun, S. Ascenzi, G. Ashton, M. Ast, S. M. Aston, P. Astone, P. Aufmuth, C. Aulbert, S. Babak, P. Bacon, M. K. M. Bader, P. T. Baker, F. Baldaccini, G. Ballardin, S. W. Ballmer, J. C. Barayoga, S. E. Barclay, B. C. Barish, D. Barker, F. Barone, B. Barr, L. Barsotti, M. Barsuglia, D. Barta, J. Bartlett, M. A. Barton, I. Bartos, R. Bassiri, A. Basti, J. C. Batch, C. Baune, V. Bavigadda, M. Bazzan, B. Behnke, M. Bejger, C. Belczynski, A. S. Bell, C. J. Bell, B. K. Berger, J. Bergman, G. Bergmann, C. P. L. Berry, D. Bersanetti, A. Bertolini, J. Betzwieser, S. Bhagwat, R. Bhandare, I. A. Bilenko, G. Billingsley, J. Birch, R. Birney, O. Birnholtz, S. Biscans, A. Bisht, M. Bitossi, C. Biwer, M. A. Bizouard, J. K. Blackburn, C. D. Blair, D. G. Blair, R. M. Blair, S. Bloemen, O. Bock, T. P. Bodiya, M. Boer, G. Bogaert, C. Bogan, A. Bohe, and P. Bojtos, LIGO Scientific Collaboration and Virgo Collaboration, "Observation of gravitational waves from a binary black hole merger," Phys. Rev. Lett. **116**, 061102 (2016).
5. R. Abuter, A. Amorim, M. Bauboeck, J. P. Berger, H. Bonnet, W. Brandner, V. Cardoso, Y. Clenet, P. T. de Zeeuw, J. Dexter, A. Eckart, F. Eisenhauer, N. M. Foerster Schreiber, P. Garcia, F. Gao, E. Gendron, R. Genzel, S. Gillessen, M. Habibi, X. Haubois, T. Henning, S. Hippler, M. Horrobin, A. Jimenez-Rosales, L. Jochum, L. Jocou, A. Kaufer, P. Kervella, S. Lacour, V. Lapeyrere, J.-B. Le Bouquin, P. Lena, M. Nowak, T. Ott, T. Paumard, K. Perraut, G. Perrin, O. Pfuhl, G. Rodriguez-Coira, J. Shangguan, S. Scheithauer, J. Stadler, O. Straub, C. Straubmeier, E. Sturm, L. J. Tacconi, F. Vincent, S. von Fellenberg, I. Waisberg, F. Widmann, E. Wieprecht, E. Wiezorrek, J. Woillez, S. Yazici, and G. Zins, and GRAVITY Collaboration, "Detection of the Schwarzschild precession in the orbit of the star S2 near the Galactic centre massive black hole," Astron. Astrophys. **636**, L5 (2020).
6. J. B. Pendry, D. Schurig, and D. R. Smith, "Controlling electromagnetic fields," Science **312**, 1780–1782 (2006).
7. U. Leonhardt, "Optical conformal mapping," Science **312**, 1777–1780 (2006).
8. H. Y. Chen, C. T. Chan, and P. Sheng, "Transformation optics and metamaterials," Nat. Mater. **9**, 387–396 (2010).
9. V. M. Shalaev, "Transforming light," Science **322**, 384–386 (2008).
10. D. Schurig, J. J. Mock, B. J. Justice, S. A. Cummer, and J. B. Pendry, "Metamaterial electromagnetic cloak at microwave frequencies," Science **314**, 977–980 (2006).
11. W. S. Cai, U. K. Chettiar, A. V. Kildishev, and V. M. Shalaev, "Optical cloaking with metamaterials," Nat. Photonics **1**, 224–227 (2007).
12. H. Y. Chen, Z. X. Liang, P. J. Yao, X. Y. Jiang, H. R. Ma, and C. T. Chan, "Extending the bandwidth of electromagnetic cloaks," Phys. Rev. B **76**, 241104 (2007).
13. R. Liu, C. Ji, J. J. Mock, J. Y. Chin, T. J. Cui, and D. R. Smith, "Broadband ground-plane cloak," Science **323**, 366–369 (2009).
14. S. Tretyakov, P. Alitalo, O. Luukkonen, and C. Simovski, "Broadband electromagnetic cloaking of long cylindrical objects," Phys. Rev. Lett. **103**, 103905 (2009).
15. J. Valentine, J. S. Li, T. Zentgraf, G. Bartal, and X. Zhang, "An optical cloak made of dielectrics," Nat. Mater. **8**, 568–571 (2009).
16. L. H. Gabrielli, J. Cardenas, C. B. Poitras, and M. Lipson, "Silicon nanostructure cloak operating at optical frequencies," Nat. Photonics **3**, 461–463 (2009).
17. I. I. Smolyaninov, V. N. Smolyaninova, A. V. Kildishev, and V. M. Shalaev, "Anisotropic metamaterials emulated by tapered waveguides: application to optical cloaking," Phys. Rev. Lett. **102**, 213901 (2009).
18. H. Y. Chen and C. T. Chan, "Transformation media that rotate electromagnetic fields," Appl. Phys. Lett. **90**, 241105 (2007).
19. H. Y. Chen, B. Hou, S. Y. Chen, X. Y. Ao, W. J. Wen, and C. T. Chan, "Design and experimental realization of a broadband transformation media field rotator at microwave frequencies," Phys. Rev. Lett. **102**, 183903 (2009).
20. Y. Lai, J. Ng, H. Y. Chen, D. Z. Han, J. J. Xiao, Z. Q. Zhang, and C. T. Chan, "Illusion optics: the optical transformation of an object into another object," Phys. Rev. Lett. **102**, 253902 (2009).
21. H. Y. Chen, R. X. Miao, and M. Li, "Transformation optics that mimics the system outside a Schwarzschild black hole," Opt. Express **18**, 15183–15188 (2010).
22. E. E. Narimanov and A. V. Kildishev, "Optical black hole: broadband omnidirectional light absorber," Appl. Phys. Lett. **95**, 041106 (2009).
23. Q. Cheng, T. J. Cui, W. X. Jiang, and B. G. Cai, "An omnidirectional electromagnetic absorber made of metamaterials," New J. Phys. **12**, 063006 (2010).
24. D. A. Genov, "Optical black-hole analogues," Nat. Photonics **5**, 76–78 (2011).
25. H. Y. Chen, S. C. Tao, J. Bělin, J. Courtial, and R. X. Miao, "Transformation cosmology," Phys. Rev. A **102**, 023528 (2020).
26. H. W. Wang and L. W. Chen, "A cylindrical optical black hole using graded index photonic crystals," J. Appl. Phys. **109**, 103104 (2011).
27. S. Y. Liu, L. Li, Z. F. Lin, H. Y. Chen, J. Zi, and C. T. Chan, "Graded index photonic hole: analytical and rigorous full wave solution," Phys. Rev. B **82**, 054204 (2010).
28. C. Sheng, R. Bekenstein, H. Liu, S. N. Zhu, and M. Segev, "Wavefront shaping through emulated curved space in waveguide settings," Nat. Commun. **7**, 10747 (2016).
29. M. Li, R. X. Miao, and Y. Pang, "Casimir energy, holographic dark energy and electromagnetic metamaterial mimicking de Sitter," Phys. Lett. B **689**, 55–59 (2010).
30. M. Li, R. X. Miao, and Y. Pang, "More studies on metamaterials mimicking de Sitter space," Opt. Express **18**, 9026–9033 (2010).
31. T. G. Mackay and A. Lakhtakia, "Towards a metamaterial simulation of a spinning cosmic string," Phys. Lett. A **374**, 2305–2308 (2010).
32. C. Sheng, H. Liu, H. Y. Chen, and S. N. Zhu, "Definite photon deflections of topological defects in metasurfaces and symmetry-breaking phase transitions with material loss," Nat. Commun. **9**, 4271 (2018).
33. J. Evans, "The ray form of Newton's law of motion," Am. J. Phys. **61**, 347–350 (1993).
34. J. Evans, "Simple forms for equations of rays in gradient-index lenses," Am. J. Phys. **58**, 773–778 (1990).
35. D. A. Genov, S. Zhang, and X. Zhang, "Mimicking celestial mechanics in metamaterials," Nat. Phys. **5**, 687–692 (2009).
36. U. Leonhardt and T. Philbin, *Geometry and Light: The Science of Invisibility* (Courier, 2012).
37. L. D. Landan and E. M. Lifshitz, *The Classical Theory of Fields, Course of Theoretical Physics* (Butterworth Heinemann, 1975), Vol. **2**.
38. H. Reissner, "Über die Eigengravitation des elektrischen Feldes nach der Einsteinschen Theorie," Ann. Phys. **355**, 106–120 (1916).
39. G. Nordström, "On the energy of the gravitation field in Einstein's theory," Proc. Kon. Ned. Akad. Wet. **20**, 1238–1245 (1918).
40. B. James and T. Scott, *Galactic Dynamics* (Princeton University, 2009).
41. J. E. Eaton, "On spherically symmetric lenses," IRE Trans. Antennas Propag. **PGAP-4**, 66–71 (1952).
42. T. Tyc, L. Herzánová, M. Šarbort, and K. Bering, "Absolute instruments and perfect imaging in geometrical optics," New J. Phys. **13**, 115004 (2011).
43. R. K. Luneburg, *Mathematical Theory of Optics* (University of California, 1964).
44. H. Y. Chen and W. Xiao, "Morse lens," Chin. Opt. Lett. **18**, 062403 (2020).